CrossMark

ORIGINAL RESEARCH

SWS

Assessing Land Cover Change and Anthropogenic Disturbance in Wetlands Using Vegetation Fractions Derived from Landsat 5 TM Imagery (1984–2010)

Laura Dingle Robertson[1] · Douglas J. King[1] · Chris Davies[2]

Abstract Anthropogenic disturbance of wetlands in Canada is extensive. In wetland monitoring programs disturbance assessment often relies on single date field and geo-spatial data, thereby rendering detection of the nature, timing and magnitude of disturbance events and trends difficult. The Landsat temporal archive provides potential for more comprehensive temporal change analysis. However, its 30 m pixel size may result in omission of small disturbances or lack of spatial precision near boundaries where change often occurs. Spectral mixture analysis (SMA) is a subpixel technique that has been used to assess change in a variety of land cover types, but rarely for non-coastal wetlands. This research utilized SMA vegetation, bare, and moisture fractions derived from 26 Landsat 5 Thematic Mapper (TM) scenes from 1984 to 2010 in two-date comparisons and time series analysis to assess disturbance in two wetland complexes in eastern Ontario. The 1984–2010 two-date analysis showed overall declines in vegetation and moisture fractions and increases in the bare fraction, while time series analysis over the 26 year period showed more variable inter-annual changes including years of sudden change, cyclic trends and more gradual trends. Anthropogenic disturbances that were identified included a lake created for recreational purposes, logged/cultivated areas, and wetland degradation due to encroaching development.

Keywords Wetlands · Spectral mixture analysis · Anthropogenic disturbance · Time series · Landsat

Introduction

Wetlands provide many ecological services, but are under threat from climate change and land modification amongst other stressors. Approximately 5 % of the world's wetlands are located in Ontario (National Wetlands Working Group 1988). Across eastern Ontario, wetland losses range from 45 to 95 %, with higher proportions near the urban centres of Kingston and Ottawa (GLWCAP 2012).

The Ontario Wetland Evaluation System (OWES) is used by the Ontario Ministry of Natural Resources (OMNR) for the evaluation of wetlands to inform land use planning (Ontario Wetland Evaluation System: Southern Manual 2013). It assesses wetland ecological functions and their social and economic values in four components: Biological, Hydrologic, Social and Special Features. These components are comprised of sub-categories and 'attributes', which are each assigned a score. With a high overall score, a wetland is designated as "significant", which facilitates the implementation of conservation policies and actions. The OWES was developed in the early 1980s and relied on field observation coupled with air photo interpretation of the attributes associated with each component. This was costly and evaluations quickly become obsolete. In the past decade, the OMNR has used GIS and remotely sensed data to assess some of these attributes. Remote sensing provides potential for wetland attribute monitoring over time and for comparison between wetlands, both not easily achieved with oblique and subjective field

✉ Laura Dingle Robertson
   lauradinglerobertson@gmail.com

   Douglas J. King
   doug.king@carleton.ca

[1] Department of Geography and Environmental Studies, Geomatics and Landscape Ecology Research Laboratory, Carleton University, Ottawa, Canada

[2] Ontario Ministry of Natural Resources, Trent University, Peterborough, Canada

🙋 Springer

interpretation (Lee and Lunetta 1995; Ramsey 1998; Ozesmi and Bauer 2002; Mitsch and Gosselink 2007). This study, in collaboration with the OMNR, was designed to develop means to detect and assess land cover change and anthropogenic disturbance in eastern Ontario wetlands. It is part of a larger project to develop remote sensing and GIS methods for assessment of 14 OWES attributes (Dingle Robertson 2014).

Anthropogenic disturbance is an attribute of the sub-category of Landscape Aesthetics under the Social component. It is concerned with human impacts (or lack thereof) on the aesthetics of a wetland (Ontario Wetland Evaluation System: Southern Manual 2002). Depending on the disturbance magnitude and spatial-temporal extent, wetland function may also be impaired. Human activities in or near wetlands that result in such impacts include: the building of roads, utility corridors, and buildings; creation of dumps; filling, channelization and dredging; creation of drainage ditches and control dams; etc. In the OWES, the areal extent of disturbances is estimated, with larger extents reducing the score.

The temporal archive of Landsat imagery surpasses all other moderate resolution satellite imagery currently available and the 185 km swath ensures that entire wetland complexes or multiple wetlands within a region can be covered. Landsat multispectral data have been used for mapping of wetland classes such as palustrine wetlands, mangroves, salt marshes, freshwater marshes, mud tide flats, etc. (e.g., Wright and Gallant 2007; Waleska et al. 2011; Zhang et al. 2012). Landsat has also been used for biophysical modelling of dead biomass, total biomass, mangrove wetland biomass, etc. with moderate precision and accuracy (e.g., Hardisky et al. 1984; Tan et al. 2003; Li et al. 2007; Rivero et al. 2007), but its spatial resolution is often too coarse for detailed vegetation change analysis. To take advantage of the Landsat temporal archive while incorporating more spatially precise detail, sub-pixel analysis techniques provide potential for detailed assessment of land cover change in and around wetland complexes. Vegetation fractions derived from spectral unmixing or, as used hereafter, spectral mixture analysis (SMA) (Rogers and Kearney 2004; Jensen 2005) have been analyzed to assess change in a variety of land cover types, successfully showing both vegetation degradation and regeneration (Sabol et al. 2002; Hostert et al. 2003; Sunderman and Weisberg 2011; Dubovyk et al. 2012). In coastal wetlands Yang et al. (2013) assessed the abundance of land cover types using SMA fractions derived from Landsat TM images for 1987, 2004, 2005 and 2006. Increasing vegetation fractions over that period were indicative of increases in low vegetation cover, while decreasing vegetation fractions indicated reduced tall vegetation cover due to Hurricane Katrina damage. Michishita et al. (2012b) used five Landsat TM-derived SMA fractions of green vegetation, non-photosynthetic

vegetation, soils and impervious surfaces, bright water and dark water from 2004 and 2005 and were able to detect rapid changes in water levels and rice farming extents in wetlands at Poyang Lake, China. Michishita et al. (2012a) used five Landsat 5 TM images from 1987 to 2009 to determine the changes in urban land cover fractions in four Chinese cities. Six land cover endmembers (EMs as defined in 3.2) of green vegetation, non-photosynthetic vegetation & soil, built-up, lake and river beds, bright water, and dark water were used with an advanced SMA, multiple endmember spectral mixture analysis (MESMA), which allows for the make-up of endmembers to vary on a pixel by pixel basis. Fraction images were derived for each EM and Land Cover Change Intensity (LCCI), and Dominant LCCI indices were calculated as the average change in area per EM type per pixel between two observation dates. Examples of other studies using unmixed Landsat fractions include: land cover change analysis based upon climatic differences over time (Schmid et al. 2005; Melendez-Pastor et al. 2010), tundra land cover change mapping (Olthof and Fraser 2007), and mapping of slash and burn anthropogenic disturbance in Amazon forests (Adams et al. 1995). Techniques of time series analyses have been widely applied in forestry-based research (e.g., Banskota et al. 2014; Czerwinski et al. 2014), however, few of these methods have been utilized for long temporal time series analysis of wetlands and were generally applied using full pixel variables such tasseled cap variables (Kayastha et al. 2012) or MODIS NDVI (Fuller and Wang 2014).

The objective of this study was to determine if SMA applied to temporal Landsat TM data can be used to identify and monitor disturbance and land cover change in and around wetlands.

Study Areas

This research was carried out in eastern Ontario, Canada (Fig. 1), a region of approximately 15,500 km^2 comprised of a mix of agricultural, forest, and urban lands including the city of Ottawa. Wetlands are common and are predominantly swamps and marshes with fewer bogs and fens (National Wetlands Working Group 1997). In the northwest and west there are many lakes, allowing for wetland formation in bays and along shores.

Criteria used to select the wetland complexes were that: 1) they must be provincially significant; 2) their size must be suitable for analysis using moderate resolution Landsat imagery; and 3) they must be comprised of three or more wetland types. Four wetland complexes met these criteria and were used in the broader study (Dingle Robertson 2014). Two of these included areas of known anthropogenic disturbance: Loch Garry Wetland Complex (hereafter 'Loch Garry'), and Westport-Nelson Wetland Complex (hereafter 'Westport').

Fig. 1 Eastern Ontario and the position of the two wetland complex study areas (*red squares*)
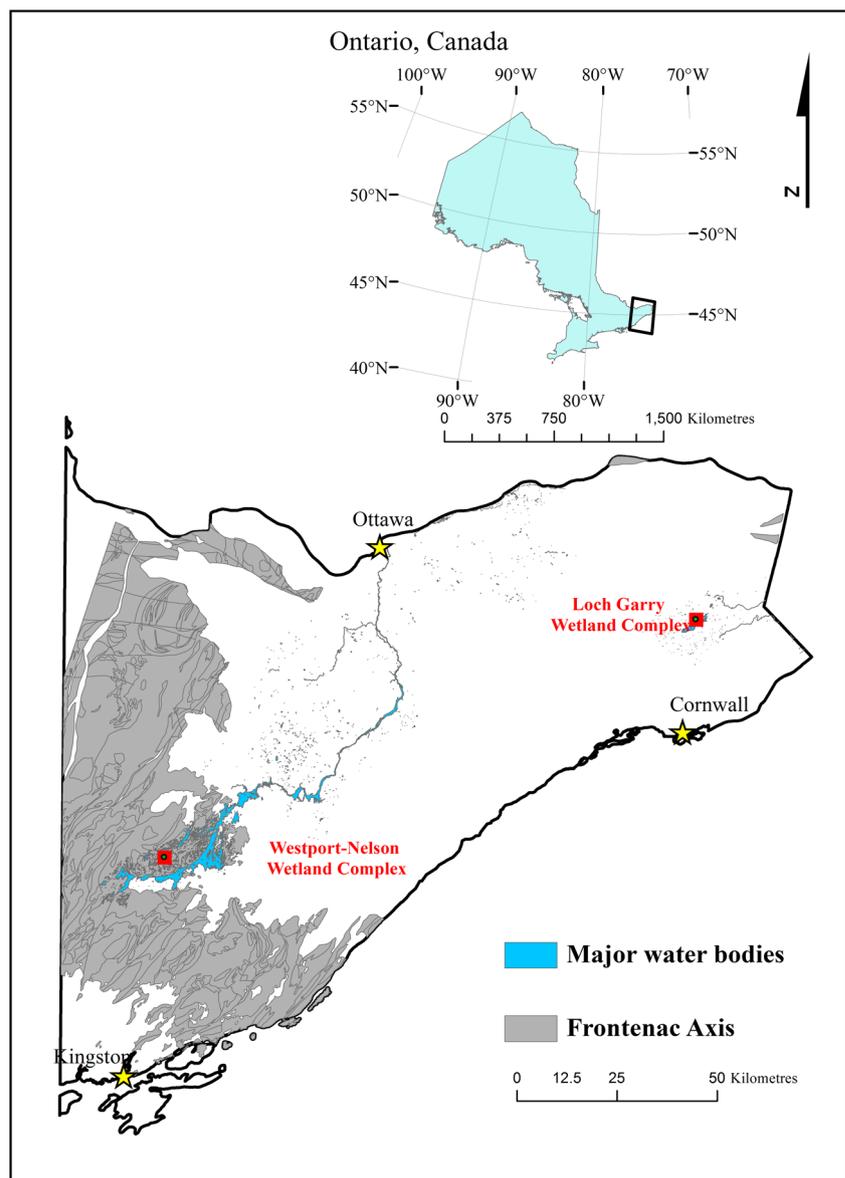
Situated within fragmented farmland north of Cornwall, Ontario, Loch Garry (Fig. 2) is the name of a both large lake as well as the wetland complex adjacent to the lake. The lake is shallow (1 to 5 m) and 380 ha (3.8 km^2) in area. The wetland complex is comprised of fen, marsh and swamp over approximately 1280 ha within the Garry River watershed (3400 ha).

Westport (Fig. 3) is located on the Frontenac Axis, approximately 120 km southwest of Ottawa. The Frontenac Axis (shaded grey in Fig. 1) is an extension of the pre-Cambrian Canadian Shield and divides the St. Lawrence lowlands to the east and the Great Lakes lowlands to the west. Bedrock is often found at the surface, or covered with thin soils (Keddy 1995; Baldwin et al. 2000). Irregular topography and marl-based ponds and lakes restrict the hydrology of the area (Keddy 1995). Wetlands present include bog, marsh and swamp with some poor fen (not observed by the authors and noted to be very rare

(Keddy 1995)). Westport and Loch Garry were last assessed in the field under the OWES in 1984.

Methods

Remotely Sensed Data Acquisition and Processing

Landsat 5 TM imagery was selected because of its long temporal archive and because it can be easily acquired at no cost. Landsat 5 continually acquired imagery using the TM instrument from 1984 until November 2011 on a 16-day revisit basis with nominal ground pixel sizes of 30 m over a 185 × 185 km area. Spectral bands used in this research included blue-green (450–520 nm), green (520–600 nm), red (630–690 nm), and near infrared (NIR, 760–900 nm), as well
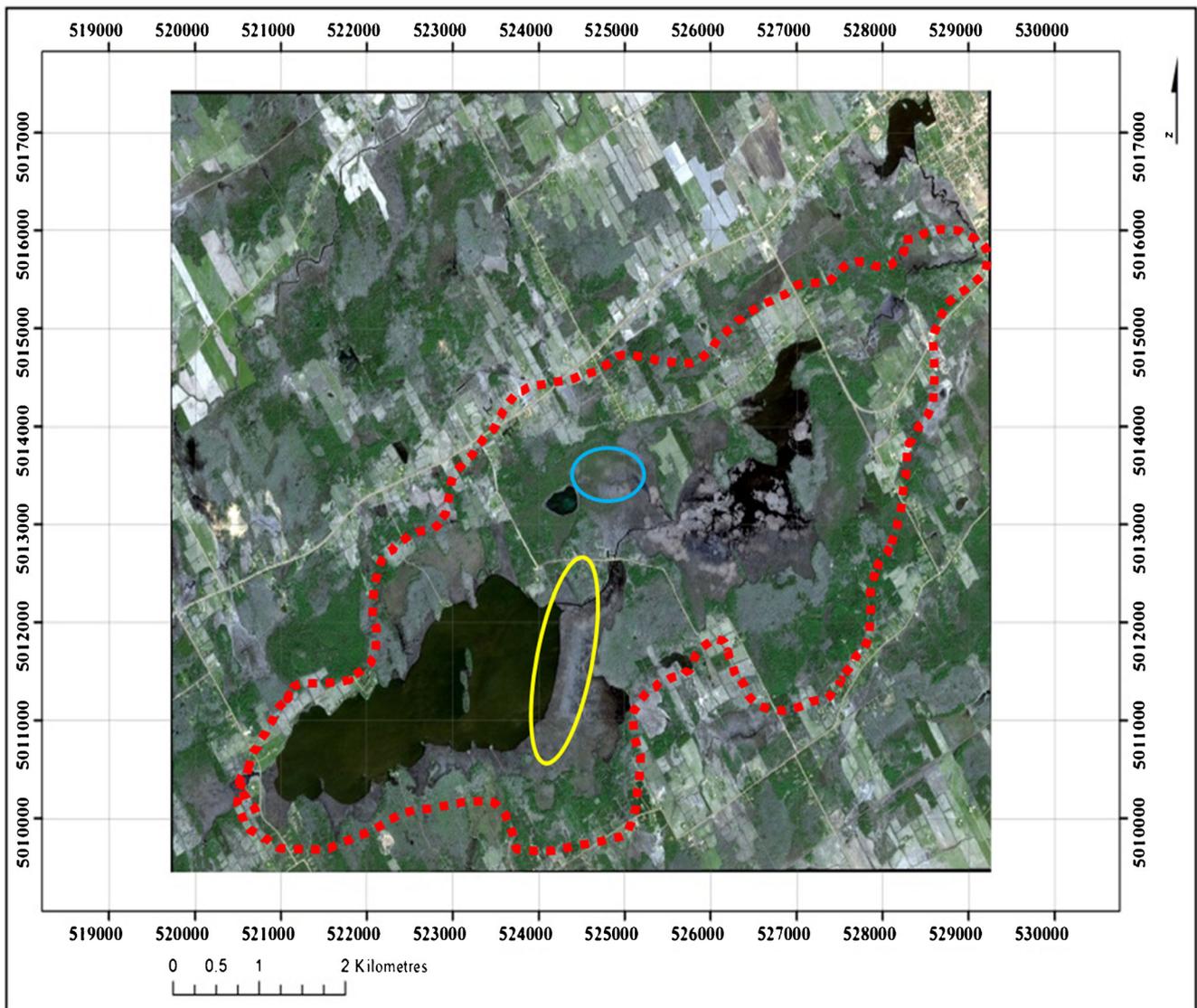
Fig. 2 2010 Landsat TM 5 true colour composite of Loch Garry wetland complex (*red dotted outline*). *Yellow* and *blue ellipse*s surround fen areas assessed as 'significant' by the OWES in 1984

as two mid-infrared (MIR) bands, MIR1 (1550–1750 nm) and MIR2 (2080-2350 nm). A cloud free Landsat 5 TM scene was acquired for August 20 1984, to align closely with the OWES field-based campaign of August 1984. A cloud-free scene was acquired for the summer of 2010, aligning with the first summer of the authors' field work. These 1984 and 2010 Landsat data were used in evaluation of two-date image comparison. Additionally, the best cloud-free summer imagery was selected for every year between the end points on a date that was near the end of summer (i.e., August-September, although as early as mid-June when data were limited), resulting in a time series of 26 scenes. Table 1 provides the dates of the acquired imagery. This time series was used in evaluation of vegetation fraction trend analysis for Westport. All images were converted to Top-of-Atmosphere (TOA) reflectance using radiometric calibration coefficients (after Chander et al. 2009) and the

images were then relatively calibrated using pseudo-invariant features (PIFs, Pax-Lenney et al. 2001; Dingle Robertson and King 2011) with the 2010 image as the master.

Spectral Mixture Analysis

For brevity SMA is not described in detail but descriptions can be found in Shimabukuro and Smith (1991); Neville et al. (1998); Rogers and Kearney (2004); Jensen (2005), among others. Spectral mixture analysis (SMA) is a technique linked to reflectance theory of linear mixing of radiance from land cover types within a pixel area (Rogers and Kearney 2004). It can be used to derive the proportion of reflectance within a pixel that can be attributed to pure surface elements of unique spectral reflectance, called endmembers (EMs - e.g., vegetation, soil, water or moisture) (Neville et al. 1998). SMA has two key processing steps: 1)
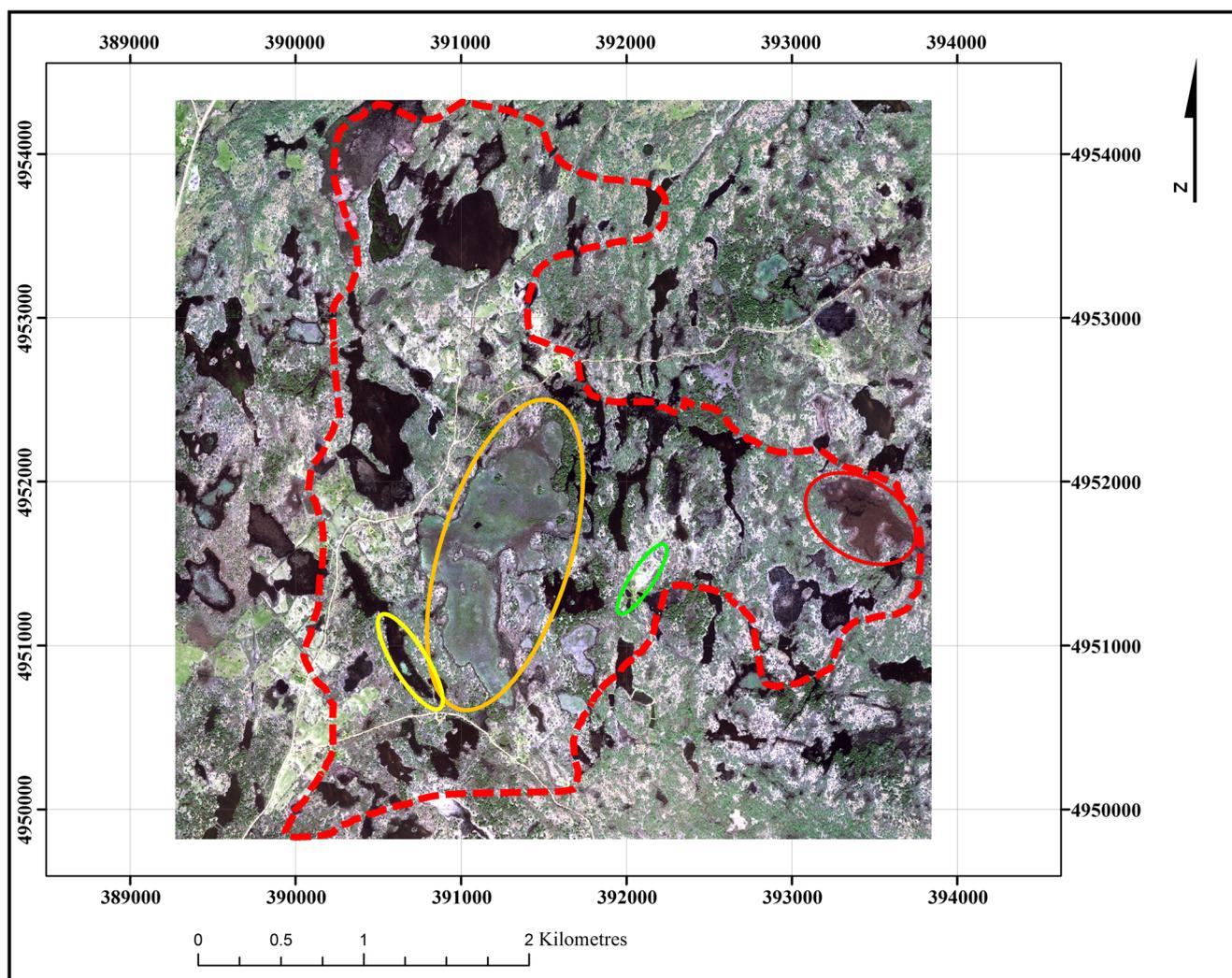
Fig. 3 2010 Landsat TM 5 true colour composite of Westport wetland complex (*red dotted outline*). *Orange ellipse* surrounds a bog assessed as 'significant' in 1984. *Yellow*, *green*, and *red ellipses* highlight areas of known change

EM development, and 2) pixel unmixing. One of the most common automated methods of EM selection that was used in this research is the iterative error analysis (IEA) algorithm as described in Neville et al. (1998).

From the location of EMs within n-dimensional spectral space, a linear mixture model is used to determine the proportion of each EM in each pixel. The Least-Squares Mixture Model (Shimabukuro and Smith 1991) defines the spectral vector of a pixel as the sum of the reflectance of each EM within that pixel plus an error term. Constrained SMA

assumes that the sum of the pixel fractions is equal to the total pixel surface; i.e., that there is no other radiance that is unaccounted for (Shimabukuro and Smith 1991).

The calibrated Landsat 5 TM images were unmixed using three automatically selected EMs representing green vegetation, moisture, and bare ground. The derived fraction maps for 1984 and 2010 for both study areas were compared using RGB image display to determine if changes related to disturbance could be observed. This is a simple process where, for a given EM type, the fraction image for the earlier date is displayed in blue and

Table 1 List of acquisition dates for Landsat 5 TM data

20–08–1984	03–08–1990	20–06–1996	03–07–2002	22–08–2008
21–09–1985	No 1991 image	19–06–1997	23–08–2003	24–09–2009
23–07–1986	11–09–1992	10–09–1998	11–09–2004	11–09–2010
11–08–1987	10–07–1993	28–08–1999	13–09–2005	
15–08–1988	30–08–1994	29–06–2000	30–07–2006	
15–07–1989	18–09–1995	01–08–2001	19–09–2007	

green, and the fraction image for the later date is displayed in red (Jensen 2005). Using the full time series of Landsat images for Westport, vegetation, soil and moisture fraction images were derived for each year and trends were graphically analysed to determine if gradual and abrupt anthropogenic change could be detected. Image processing was completed with PCI Geomatica (EM development, two-date analysis); ENVI 5.0 (EM development, pixel unmixing and time series display); and IDRISI TerrSet (pixel unmixing and time series analysis).

Validation Data

In the spring and summer of 2010 and 2011, validation sites of approximately 90 × 90 m were established to develop understanding of the wetland composition and configuration. Thirty-one wetland and twenty-nine upland locations were visited including five fen, six marsh and six swamp sites at Loch Garry, and five bog and nine marsh sites at Westport. Additionally, local experts at Westport were interviewed to determine if there was any known anthropogenic disturbance that may have occurred in the study area.

Results

Figures 4 and 5 are the three EMs derived for the 1984 image and the 2010 image and used in the unmixing process. For all graphs the green EM values followed typical vegetation spectral reflectance curves with low blue and red reflectance, a small peak in the green band, high NIR reflectance and moderate MIR reflectance. Also, as expected, Bare EM reflectance was higher in the visible bands with lower values in the NIR and MIR, and moisture EM reflectance was low across all spectral bands.
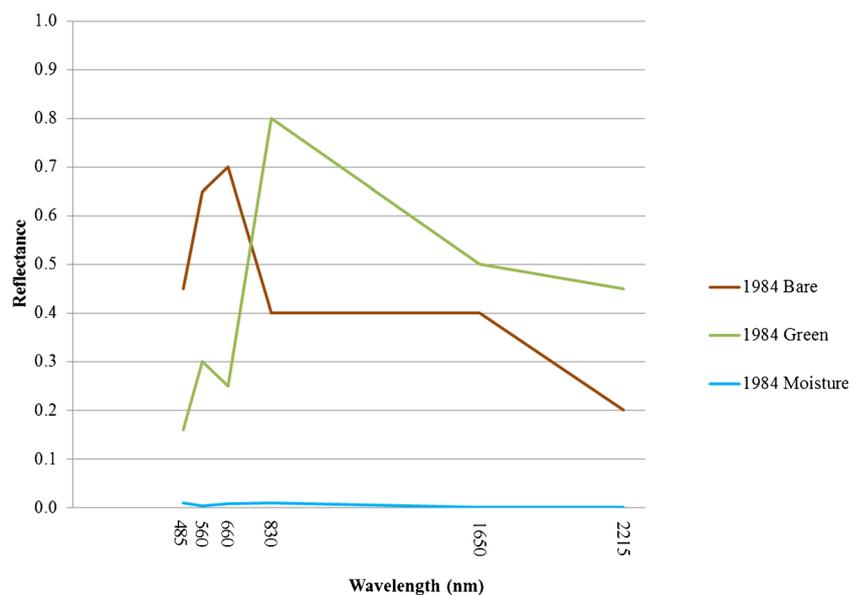
Loch Garry: Two-Date Temporal Difference Analysis

Figure 6 shows the combined 1984/2010 RGB fraction change images for Loch Garry.

Areas of similarly high vegetation fractions (light grey/white areas) and low bare fractions (dark/black) for both years are visible in upland areas in the upper and right parts of each image and in other areas within the complex. Small areas (red circles) with higher vegetation fractions and lower moisture fractions in 2010 than in 1984 are mostly marsh. Total precipitation accumulated to September 11, 2010 was 572.1 mm and the lake water level was 89.08 m ASL (Environment Canada 2013; Loch Garry Lake Association 2012). The total precipitation accumulated to August 20, 1984 was 442.9 mm (1984 water levels are unavailable). The higher 2010 vegetation and lower moisture fractions may simply reflect with more precipitation having accumulated by the time of image acquisition in 2010 than in 1984, which may have resulted in more vegetation growth. However, more detailed analysis using time series data for the Westport study area below contradicts this hypothesis, and shows no correlation of precipitation increase with vegetation fraction increase.

Within the yellow and blue ellipses on Fig. 6 (and Fig. 2), the vegetation fractions for both years were similarly low, while the bare fractions were high. The blue circled area was visited on July 13, 2010 (Fig. 7d, e; May and July, 2010, respectively) and identified as a fen floating on water, but it was not physically possible to enter the area highlighted by the yellow ellipse. Land cover classification of both areas (see Dingle Robertson 2014) showed the wetland type was fen with 5 % open water. July 27, 2010 Worldview-2 imagery (Fig. 7a–c) distinctly shows low NIR reflectance in both areas as compared to the high NIR reflectance of the surrounding

Fig. 4 TOA spectral reflectance for three EMs from 1984 Landsat 5 TM imagery

Fig. 5 TOA spectral reflectance for three EMs from 2010 Landsat 5 TM imagery
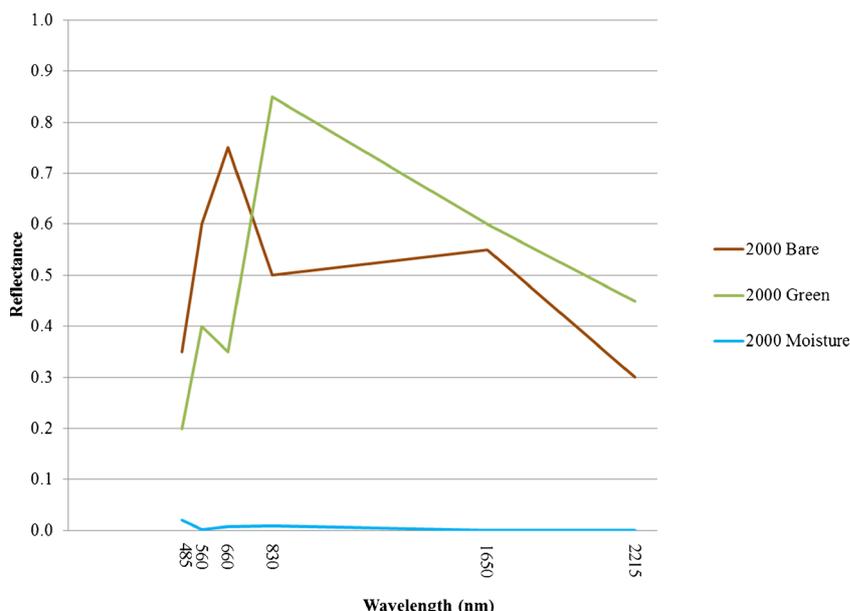
upland vegetation. From these observations, it is concluded that both areas are the same floating fen vegetation, which produces low SMA vegetation fractions. The high bare fraction values are created by a combination of senescent vegetation and the underlying mat of lightly decomposing peat. By August 20 1984, and certainly by September 11, 2010, a high proportion of the fen vegetation would typically be senescent (yellow-brown). The near vertical sensor view angle detects radiance from such senescent vegetation along with the underlying saturated peat mat radiance and these two sources dominate the signal compared to contributions from green

vegetation and standing water. Thus, for such short vegetation such as this, the EM identified as "Bare" from the SMA results could be re-labelled as Bare + Senescent Vegetation. Alternatively, a fourth EM identified as senescent vegetation may prove useful for such land cover types.

Westport: Two-Date Temporal Difference and Time Series Analyses

Two-date temporal difference analysis was conducted for the Westport wetland complex as presented above for Loch Garry. In addition, time series graphical analysis was conducted to compare the relative utility of analyses of two scenes as compared to multiple scenes for wetlands.

Figure 8 shows a portion of the Westport wetland complex using the same type of two-date colour composite for the 1984 and 2010 vegetation fractions as in Fig. 6 for Loch Garry. The orange circle delineates a bog classified in 1984 as 'significant'. Overall it is a medium grey with some cyan colour indicating moderate vegetation fractions that may have been slightly higher in 1984 than in 2010. The yellow ellipse in Fig. 8 shows a bright linear feature that represents the lower portion of a lake where vegetation fractions were higher in 1984 than in 2010. A landowner stated that flowing water had been purposefully dammed for recreational purposes, extending the linear water body to a current size of approximately 1.1 km × 0.1 km. This type of change would be considered anthropogenic disturbance within the current OWES. This feature was visually discernable because of the large magnitude of change from vegetation to water, and because of its linear shape and relatively long length. However, its small
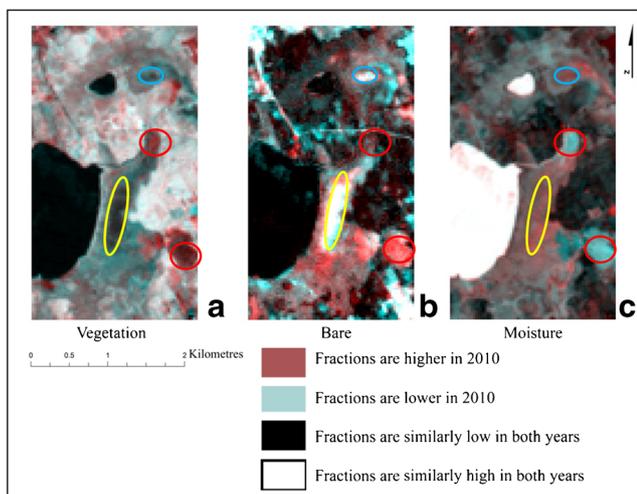
Fig. 6 Fraction images from 1984 and 2010 for Loch Garry. RGB display colours are as follows: *Red* - 2010; *Green* - 1984; *Blue* - 1984. *Yellow* and *blue ellipses* highlight areas which, for both years, had high bare fraction and low vegetation fraction. *Red circles* highlight areas where the vegetation fraction was higher and the moisture fraction was lower in 2010

Fig. 7 a July 27, 2010
WorldView-2 CIR composite for
Loch Garry; **b** close up of fen area
that was observed in 2010 (*blue
circle*); **c** close up of inaccessible
area (*yellow ellipse*); **d**, **e** field
photos (May and July, 2010) from
blue circle area; (*yellow dashed
line* in **c** shows the approximate
edge separating fen (*left of line*)
and forest (*right of line*))
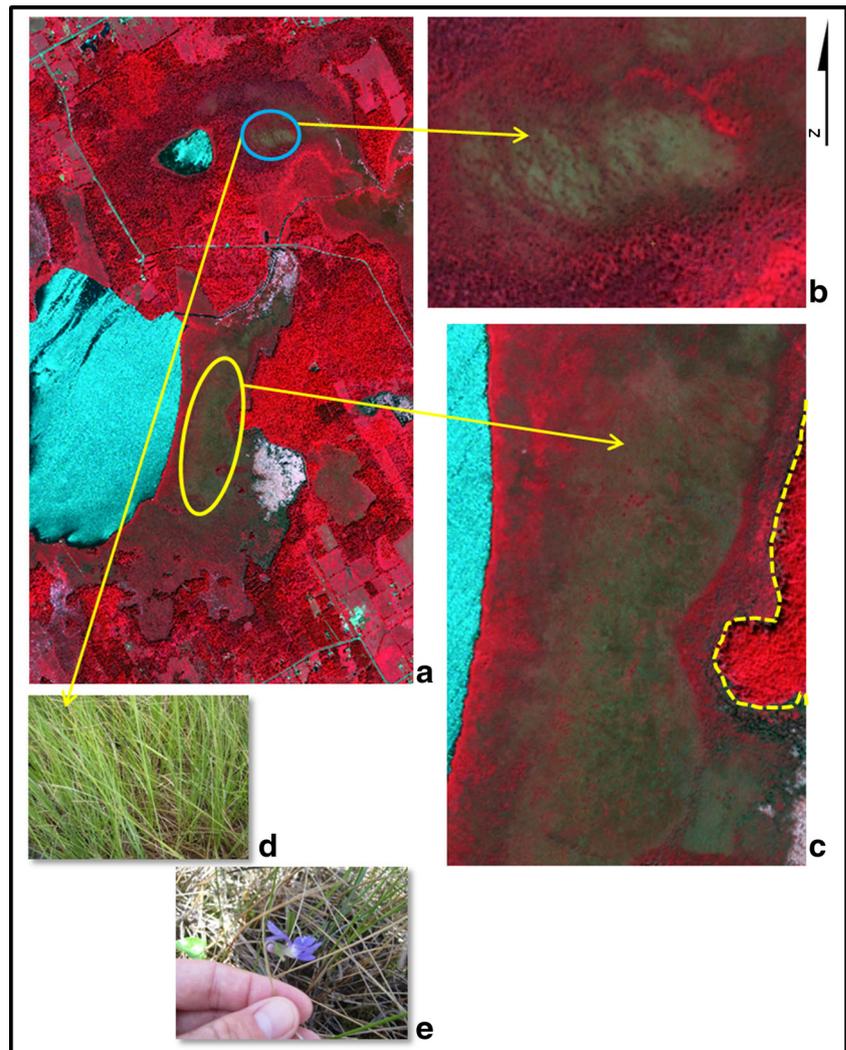
width is close to the limit of detectability for Landsat multi-spectral bands using SMA.

The time series for the dammed lake (yellow ellipse in Fig. 8) had an expected profile (Fig. 9) showing a sudden change from vegetation to water. Such time series profiles can be used to detect the year of change, in this case being between the imagery acquisition in 1984 and 1985 (vegetation fraction declined from ~70 % to less than 20 %), whereas a two-date analysis cannot. Following 1985, the vegetation fractions remained relatively low, with a few small spikes to about 40 % between 1987 and 2004. There was no relationship between the dips and peaks of the data and image acquisition DOY differences (e.g. for peaks in 1987 and 2002, the images were acquired August 11 and July 3, respectively; for the dips in 1988 and 1993, the images were acquired Aug. 15 and July 10, respectively).

Figure 10 is the time series for three larger lakes (A, B, and C on Fig. 8) that showed higher vegetation fractions in 1984

than in 2010. Each series shows significant variability in vegetation fraction from year to year that, as above, is not related to the image DOY. All three lakes experienced a drop in vegetation fractions from 1984 to 1985, similar to the dammed lake, and vegetation fractions of lake C remained low (like the dammed lake) for the remaining period of 1985–2010, with minor fluctuations. However, more importantly, each of the profiles of lakes A-C show the same general trends over the 1984–2010 period that can be separated into four sections: 1984–1993, decreasing vegetation; 1994–1998, increasing vegetation; 1998–2007, decreasing vegetation; and 2007–2010, increasing vegetation (lakes B and C only). Consequently, Pearson correlations (r) for vegetation fraction between each pair of lakes (A, B, C, dammed lake) were significant ($p < 0.05$; $n = 0.26$), ranging from 0.50 to 0.86. These trends are punctuated by deviations in various years that add noise to the overall cyclic trend. Lakes A and B have the highest overall vegetation fractions throughout the time series

Fig. 8 Temporal composite of 1984 and 2010 vegetation fractions for Westport. RGB display colours are: *Red* - 2010; *Green* - 1984; *Blue* - 1984. The *yellow ellipse* and letters *A, B, C* indicate areas with higher vegetation fractions in 1984; the red and green ellipses highlight areas with higher vegetation fractions in 2010. *Orange ellipse* surrounds the 'significant' bog
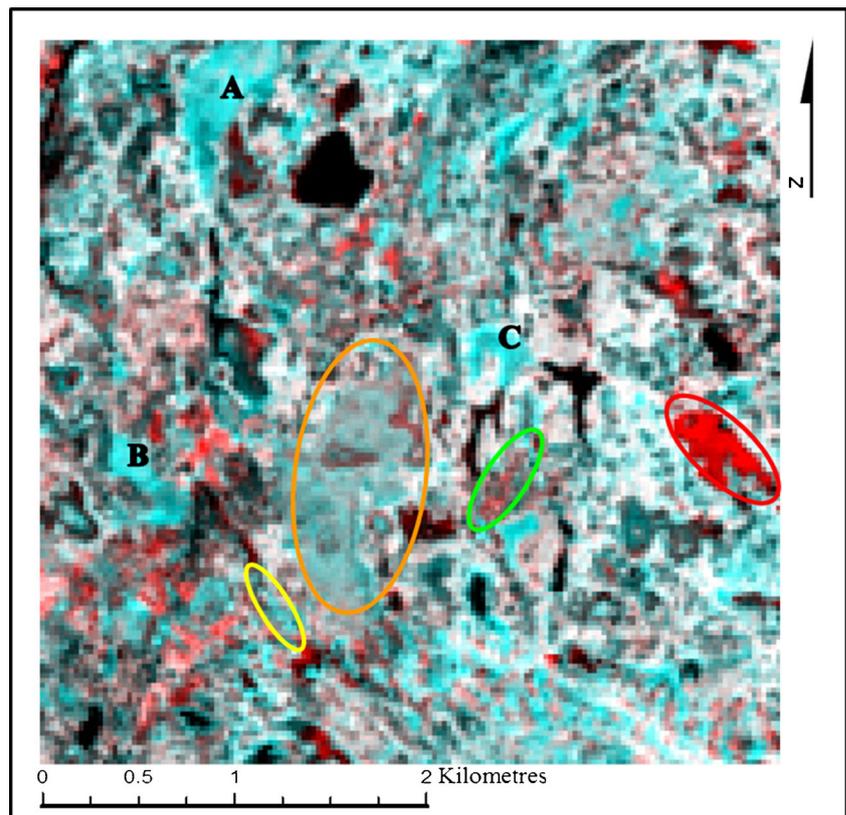
and each peaks at different times within this period. For example, lake A had four very large peaks in 1984, 1990, 1996 and 1998 and two very low vegetation fractions in 1988 (12 %) and 2008 (22 %). Lake C had lower vegetation fractions than lakes A and B; it also had low temporal fluctuations similar to those of the dammed lake. Overall, these lake time series show how variable wetland vegetation fractions can be both inter-annually and over longer cycles. Detailed climate data for the area were evaluated (Fig. 10) to determine if these lakes' vegetation fraction dynamics are related to precipitation or temperature. The hypotheses were that wetter and/or warmer conditions are related to increased vegetation fraction in these lakes. Total precipitation in the year (from January 1) leading up to image acquisition and precipitation in the 30 days prior to image acquisition were assessed. For temperature, the mean maximum daily temperature for the month of image acquisition (°C) was assessed. No significant relationships were found ($p < 0.05$; $r = -0.07$–0.33), leading to the conclusion that lake vegetation fraction is not strongly related to monthly temperature and cumulative precipitation. If other data such as fertilizer use on nearby farms were available they might provide some insight into these inter-annual variations in lake vegetation fraction but such data did not exist.

The red ellipse in Fig. 8 (and Fig. 3) highlights an area with higher vegetation fractions in 2010 than in 1984. In 1984, based on its very low reflectance across the visible, NIR and MIR, this area was obviously a lake. In 2010, as shown in the natural colour composite of Fig. 3, it is still evident as a lake (red ellipse), but the water within the ellipse is brighter than many other lakes, indicating the presence of surface vegetation. The 2010 WorldView-2 CIR composite (Fig. 11d) confirms the presence of this surface vegetation, which was not present in 1984 and is not similar to the other lakes (e.g. A, B, and C) in the study area. Figure 11 shows the time series profiles for the average vegetation, bare and moisture fractions for this lake for images with acquisition dates of July 15th onward (i.e., when vegetation would be expected to develop). Between 1992 and 1995, a very significant change occurred, which resulted in all subsequent years having large vegetation fractions. This is further supported by Fig. 12, which shows a close up of the same lake in spring 2010 from a WorldView-2 CIR composite. Surface or near surface vegetation is evident even in spring, and channels are apparent that cut through the vegetation. These data show that this lake has changed from open water to a wetland and that the change began quite suddenly over a period of 1–3 years. Such a change is important for an evaluation system like the OWES which evaluates both existing and new Ontario wetlands.

The green circle in Fig. 8 (and Fig 3) is shown in a zoomed-in image in Fig. 13. Its red colour in Fig. 13 shows that this is another area with higher vegetation fractions in 2010 than in 1984. The summer 2010 WorldView-2 CIR composite shows that this area is subject to land uses that would result in temporally dynamic reflectance. In contrast to changes discussed
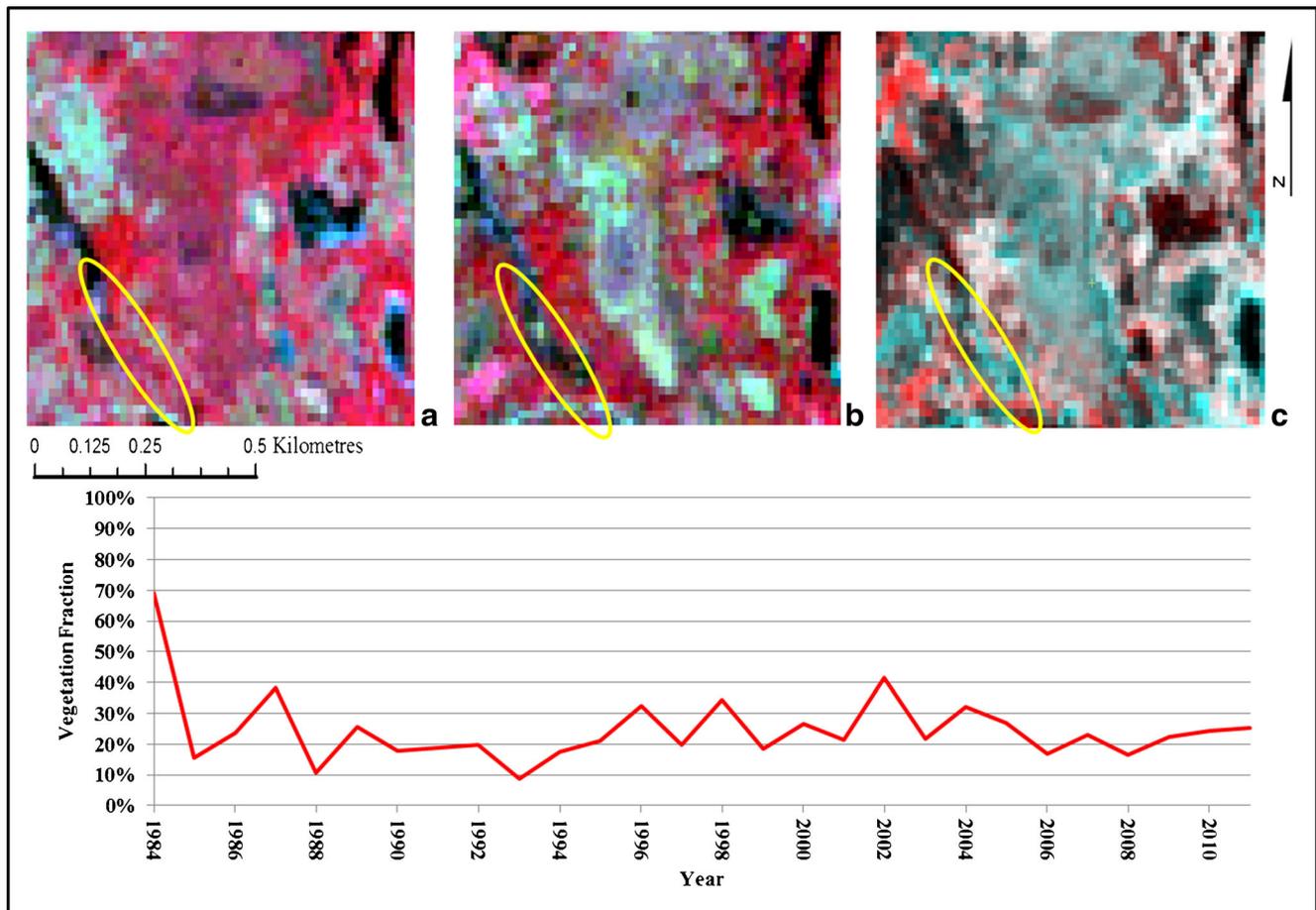
Fig. 9 Time series profile (*red line* in graph) of vegetation fraction values for a polygon within the central portion of the linear dammed area (vegetation changed to water) at Westport. **a** 1984 CIR Landsat composite; **b** 2010 Landsat CIR composite; **c** vegetation fraction composite (*Red* - 2010; *Green* - 1984; *Blue* - 1984)

previously for other features, the time series for the vegetation, bare and moisture fractions for this area do not show sudden changes. Instead, a repeating pattern is evident, particularly in the vegetation fraction series. This 8 to 10 year pattern may be indicative of some kind of harvesting/replanting regime. This is important to the OWES for two reasons: 1) recovery from anthropogenic disturbance would change the overall aesthetic value of a wetland, and 2) these changes occurred very close to the 'significant' bog (Fig. 3). Such anthropogenic change in proximity to provincially significant wetlands must be carefully monitored; easily accessible Landsat time series data, combined with straightforward processing such as SMA provides that potential.

Discussion

This research showed that wetland land cover change can be observed in the eastern Ontario region using Landsat imagery and SMA fractions. The remaining wetlands in Ontario are experiencing land cover change impacts, and these types of

analyses can contribute to monitoring of wetlands within the OWES. The long temporal archive of Landsat and its extensive spatial coverage allow for SMA land cover change and trend analysis over a provincial region to be conducted at very low cost. These capabilities make this an attractive approach for an operational evaluation and monitoring system, particularly as an alternative to costly acquisition of a higher resolution imagery. This two-date and time series analyses showed the utility of the Landsat data base for identifying specific points in time of sudden change (Figs. 9 and 11); spatial patterns and differences (Fig. 10); and overall temporal patterns (Fig. 13).

With two-date analyses, overall vegetation fractions were lower in 2010 than 1984 (except for a few marsh areas), bare fractions were higher, and moisture fractions were lower (except for fen areas) in both wetland areas. Melendez-Pastor et al. (2010) were also able to show change between two dates (2001 and 2005) for three fractions of soil, vegetation and water around an artificial wetland area. They were able to attribute the change to known drought. In the case of this research, changes between the two dates were not attributable
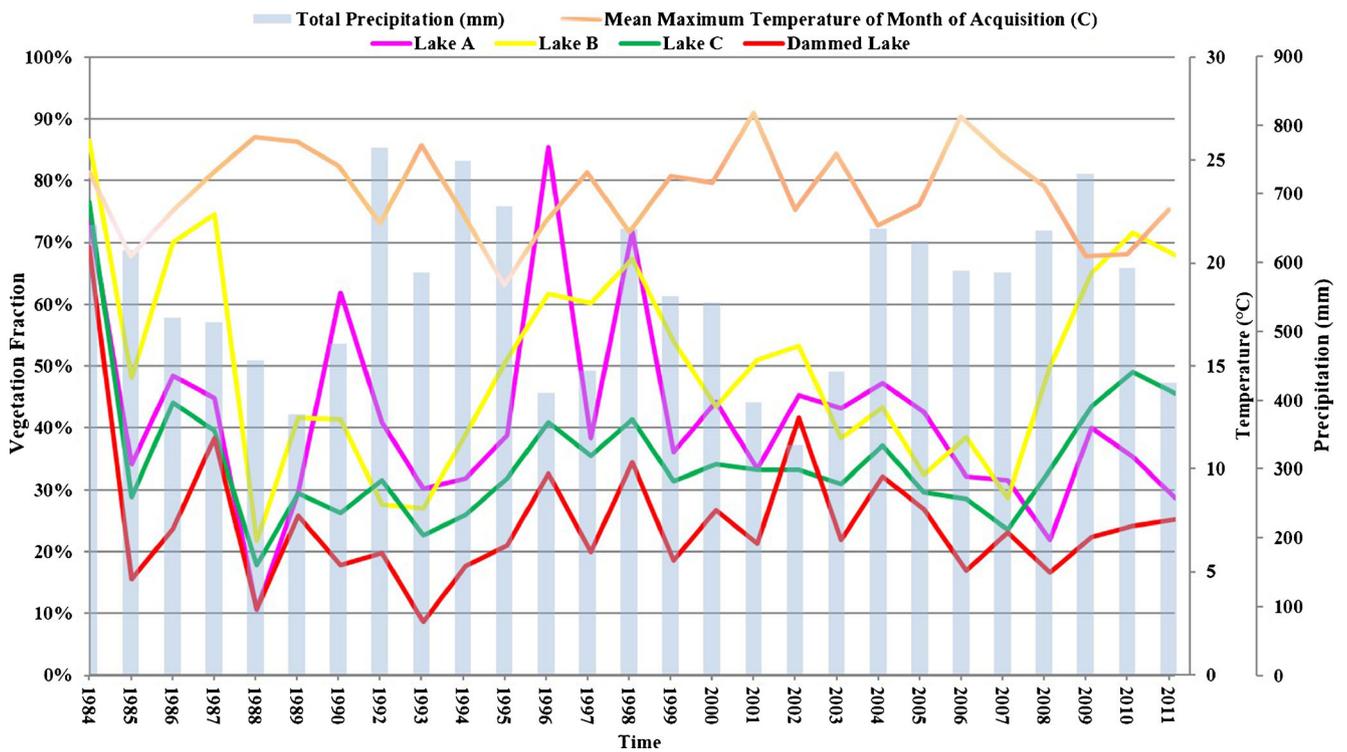
Fig. 10 Time series profile of vegetation fractions for dammed area (vegetation to water, *red line*), and three other lakes (Fig. 8, letters *A*, *B*, *C*) and climate data (total precipitation (mm) to date of image acquisition and mean maximum temperature of month of acquisition (°C)
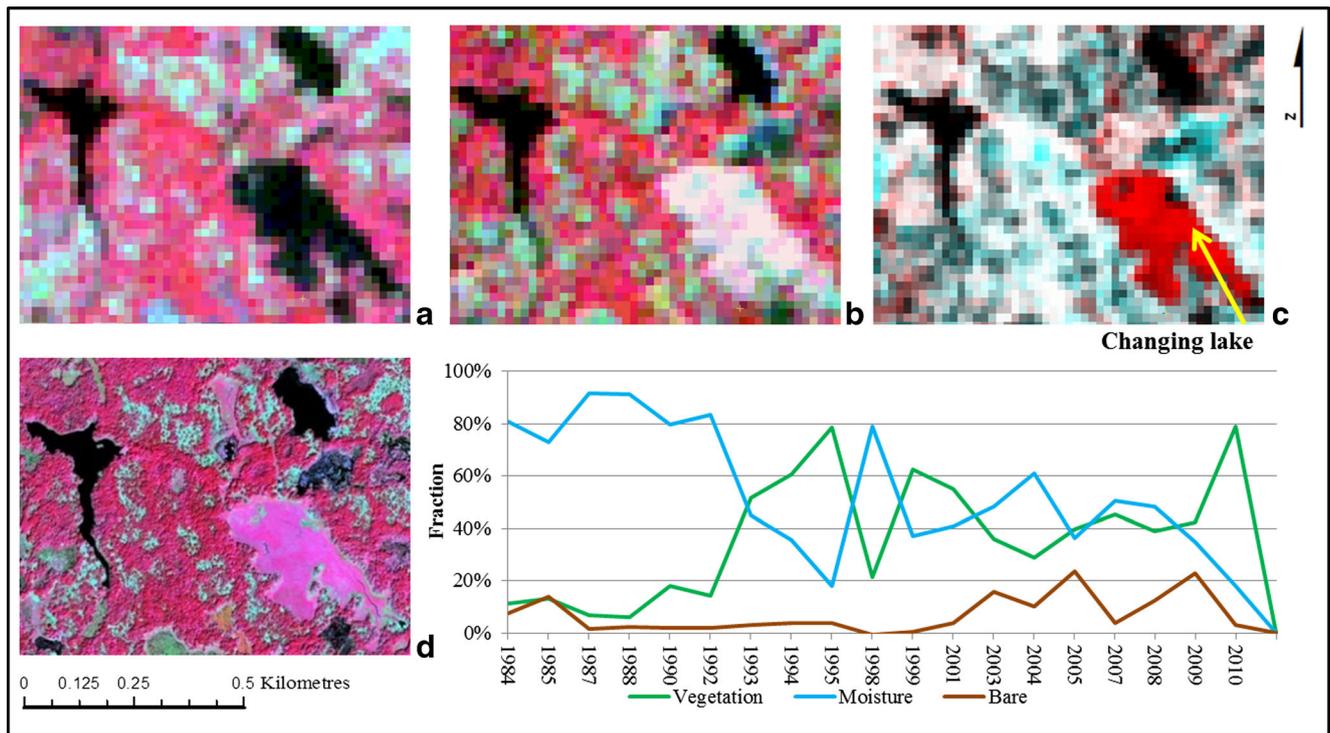
Fig. 11 Time series profiles of vegetation, moisture and bare fractions for a Westport lake. The water body changed from consistently low vegetation fractions and high moisture fractions (1984 to 1992) to high vegetation fractions and low moisture fractions (1994 to 2011). **a** 1984 Landsat CIR composite; **b** 2010 Landsat CIR composite; **c** vegetation fraction composite (*Red* - 2010; *Green* - 1984; *Blue* - 1984); and **d** 2010 summer WorldView-2 CIR composite

Fig. 12 2010 springWorldView-2 CIR composite of a lake that has changed to a wetland as presented in Fig. 11. Surface vegetation and internal drainage channels are apparent
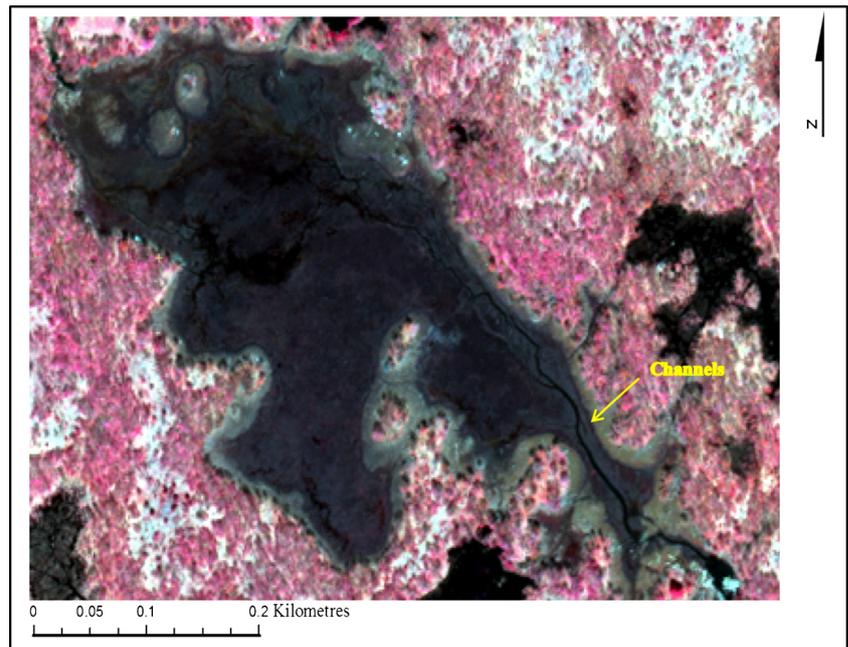
to inter-annual climatic variations, and therefore further investigation of the overall change through the whole time period is warranted. Michishita et al. (2012a) were also able to detect rapid changes in water levels and rice farming in wetlands at Poyang Lake, China using Landsat TM-derived unmixed fractions although they utilized five images to determine the types of changes, compared to the 26 scenes used in the research.

Making a definitive statement regarding long term vegetation fraction change based only on two-date imagery can be misleading. This was reinforced using the time series profile in Fig. 11, which showed that change from open lake to wetland, which was assumed to be gradual using the two-date analysis, was sudden and occurred over a three year period. The cause of this should be investigated and may include

Fig. 13 Time series profile of fraction values of human-altered area; green circle in Fig. 8. *Green line* shows the vegetation fraction; *blue line* shows the moisture fraction; *brown line* shows the bare fraction. **a** Vegetation fraction composite (*Red* - 2010; *Green* - 1984; *Blue* - 1984); and **b** summer 2010 WorldView-2 CIR composite
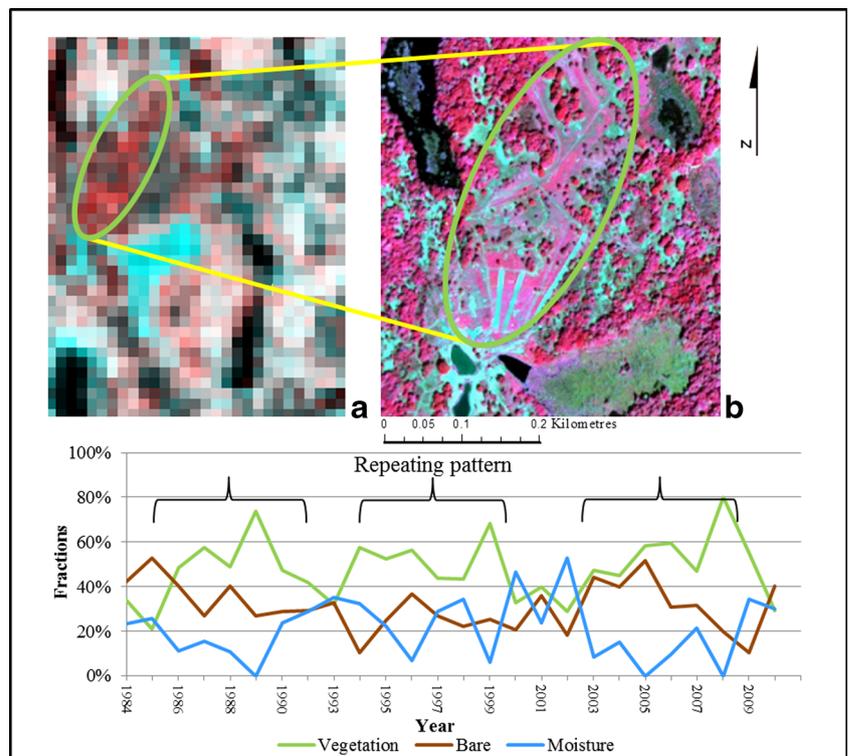
increased use of fertilizer in adjacent farms, perhaps due to a cropping change or farm expansion, or it may be partly due to a temperature/nutrient threshold linked to climate warming. Such increased lake eutrophication is currently an important topic of research in this region as it impacts ecological services provided by wetlands and water bodies (e.g., water quality and biodiversity (Albert et al. 2010; Vermaire et al. 2011)).

Confirmation of change as natural or anthropogenic can sometimes be made from the Landsat imagery itself, but often detected change areas need field verification or analysis with higher resolution imagery or field assessment at targeted locations. For example, flooding of an area for recreational purposes in Westport (yellow ellipse, Fig. 8), which produced a single significant change in the vegetation fraction during the 26 year period could be observed by comparing the two-date vegetation fraction images. By utilizing the time series profile, further insight into the timing of the change from vegetation to water (1985) and the ongoing vegetation-water dynamics was achieved. Utilizing the two-date comparison, three other lakes showing fraction changes were identified and with the time series analysis the types of change and temporal dynamics could be further assessed.

Other types of change within different land covers in inaccessible areas can also be assessed and highlighted. For example, for Fig. 13 the increasing vegetation fraction in 2010 was indicative of recovery from historical change (human altered lands, e.g. logging/pasture/agriculture). The two-date analysis did not provide insight into a particular change date, however the vegetation fraction series revealed a repeating 8 to 10-year pattern which could be related to a particular human process (e.g. logging with logging debris, new saplings and seedlings; or agriculture with rotating crop and pasture processes) resulting in a variable, but cyclic pattern. These types of time series patterns have been utilized for wetlands through vegetation and phenology indices (e.g. Normalized Difference Vegetation Index (NDVI)) (Zoffoli et al. 2008; Dong et al. 2015) and with coarser imagery types (e.g. MODIS, AVHRR) (Pekel et al. 2014), but not with fraction images.

Limitations

Difficulties in detecting short grass with strong senescent vegetation, soil, and/or water radiance contributions (e.g. fen areas, Fig. 7) as high vegetation fraction was a limitation of using three automatically generated EMs from Landsat imagery. The generalized nature of the three fractions of moisture, vegetation and soil did not take into consideration the potential for different, more mixed land cover spectral reflectance. A 4th EM could have been extracted to represent such brown-yellow reflectance typical of senescent vegetation, but it did not form a distinct vertex in the multispectral data distributions compared to vegetation, bare areas, and water. However, it may be worthwhile to implement a more advanced EM

extraction approach such as MESMA (Michishita et al. 2012a, b), with a greater number of endmembers to explore possibilities for more refined EM generation.

Small features of large change magnitude (e.g. vegetation to water), while visually apparent in the two-date change imagery (e.g. linear lake, Fig. 9), were at the limit of detectability of change. In the OWES, the score for the aesthetic sub-category is reduced more with increasing size of disturbance extent, however, smaller areas with significant change magnitude may impair wetland function (e.g. such as water quality, flood attenuation, etc. or fauna habitat for connectivity, breeding, movement, etc. (Semlitsch and Bodie 1998; Mitsch and Hernandez 2013), particularly if they are numerous. It is important to continue to assess what is the smallest possible areal extent and configuration that is detectable using a temporally robust database such as Landsat, and utilize the accumulating temporal archives of other higher resolution imagery.

Conclusions

Through the use of Landsat 5 TM and SMA vegetation, bare and moisture fractions in two-date and time series analyses, specific land cover changes and anthropogenic disturbances as well as the timing of the changes were detected. Fraction time series data provide additional insight into the types of changes that occurred over simply comparing two image dates. Overall, this research revealed the cost-effective potential for the use of time series analysis of unmixed fractions for wetland attribute monitoring, such as anthropogenic disturbance, in a regional evaluation system like the OWES.

References

Adams JB, Sabol DE, Kapos V, Almeida Filho R, Roberts DA, Smith MO, Gillespie AR (1995) Classification of multispectral images based on fractions of endmembers: application to land-cover change in the Brazilian Amazon. Remote Sensing of Environment 52:137–154

Albert MR, Chen G, MacDonald GK (2010) Phosphorus and land-use changes are significant drivers of cladoceran community composition and diversity: an analysis over spatial and temporal scales. Canadian Journal of Fisheries and Aquatic Sciences 67:1262–1273

Baldwin DJB, Desloges JR, Band LE (2000) Physical geography of Ontario. In: Perera AH, Euler DL, Thompson ID (eds) Ecology of a managed terrestrial landscape: patterns and process of forest landscapes in Ontario. British Columbia: University of British Columbia Press, Vancouver, pp. 13–29 336p

Banskota A, Kayastha N, Falkowski MJ, Wulder MA, Froese RE, White JC (2014) Forest Monitoring Using Landsat Time Series Data: A Review. Canadian Journal of Remote Sensing 40:362–384

Chander G, Markham BL, Helder DL (2009) Summary of current radiometric calibration coefficients for Landsat MSS, TM, ETM+ and EO-1 ALI sensors. Remote Sensing of Environment 113:893–903

Czerwinski CJ, King DJ, Mitchell SW (2014) Mapping forest growth and decline in a temperate mixed forest using temporal trend analysis of Landsat imagery, 1987–2010. Remote Sensing of Environment 141: 188–200

Dingle Robertson L (2014) Evaluating spatial and seasonal variability of wetlands in Eastern Ontario using remote sensing and GIS. Dissertation. Carleton University, Ottawa. 428pp

Dingle Robertson L, King DJ (2011) Comparison of pixel- and object-based classification in land cover change mapping. International Journal of Remote Sensing 32:1505–1529

Dong J, Xiao X, Kou W, Qin Y, Zhang G, Li L, Jin C, Zhou Y, Wang J, Biradar C, Liu J, Moore III B (2015) Tracking the dynamics of paddy rice planting area in 1986–2010 through time series Landsat images and phenology-based algorithms. Remote Sensing of Environment 160:99–113

Dubovyk O, Menz G, Conrand C, Khamzina A (2012) Object-based cropland degradation identification: a case study in Uzbekistan. In: Civco DL, Ehlers M, Habib S, Maltese A, Messinger D, Michel U, Nikolakopoulos KG, Schulz K (eds). Earth resources and environmental remote sensing/GIS applications III, Proc. of SPIE Vol. 8538

Environment Canada (2013) Precipitation data. http://climateweathergcca/ Date last updated: November 2013. Accessed June 2015

Fuller DO, Wang Y (2014) Recent trends in satellite vegetation index observations indicate decreasing vegetation biomass in the southeastern saline Everglades wetlands. Wetlands 34:67–77

GLWCAP (2012) Great lakes wetlands conservation action plan highlights report 2005–2010. Peterborough. 36p

Hardisky MA, Daiber FC, Roman CT, Klemas V (1984) Remote sensing of biomass and annual net aerial primary productivity of a salt marsh. Remote Sensing of Environment 16:91–106

Hostert P, Roder A, Hill J, Udelhoven T, Tsiourlis G (2003) Retrospective studies of grazing-induced land degradation: a case study in central Crete, Greece. International Journal of Remote Sensing 24:4019–4034

Jensen JR (2005) Introductory digital image processing: a remote sensing perspective. Pearson Prentice Hall, New Jersey 526p

Kayastha N, Thomas V, Galbraith J, Banskota A (2012) Monitoring wetland change using inter-annual Landsat time-series data. Wetlands 32:1149–1162

Keddy C (1995) The conservation potential of the Frontenac Axis: linking Algonquin Park to the Adirondacks. The Canadian Parks and Wilderness Society, Ottawa Valley Chapter 59p

Lee KH, Lunetta RS (1995) Wetlands detection methods. In: Lyon JG, McCarthy J (eds) Wetland and environmental applications of GIS. CRC Lewis Publishers, New York 373p

Li X, Gar-On Yeh A, Wang S, Liu K, Liu X, Qian J, Chen X (2007) Regression and analytical models for estimating mangrove wetland biomass in South China using Radarsat images. International Journal of Remote Sensing 28:5567–5582

Loch Garry Lake Association. (2012) http://www.lochgarrylakeassociation.ca/. Date last updated: 2012. Accessed Nov 2013

Melendez-Pastor I, Navarro-Pedreno J, Gomez I, Koch M (2010) Detecting drought induced environmental changes in a Mediterranean wetland by remote sensing. Applied Geography 30: 254–262

Michishita R, Jeng Z, Xu B (2012a) Monitoring two decades of urbanization in the Poyang Lake area, China through spectral unmixing. Remote Sensing of Environment 117:3–18

Michishita R, Jiang Z, Gong P, Xu B (2012b) Bi-scale analysis of multitemporal land cover fractions for wetland vegetation mapping. ISPRS Journal of Photogrammetry and Remote Sensing 72:1–15

Mitsch WJ, Gosselink JG (2007) Wetlands. Wiley, Hoboken 582 p

Mitsch WJ, Hernandez ME (2013) Landscape and climate change threats to wetlands of north and central America. Aquatic Sciences 75:133–149

National Wetlands Working Group (1988) Wetlands of Canada. Ecological land classification Series No. 24. Sustainable Development Branch, Environment Canada, Ottawa, Ontario, and Polyscience Publications Inc., Montreal. 452p

National Wetlands Working Group (1997) The Canadian Wetland Classification System, 2nd edn. In: Warner B.G. and Rubec C.D.A. (eds). Wetlands Research Centre, University of Waterloo, Waterloo, Ontario. 68p

Neville RA, Nadeau C, Levesque J, Szeredi T, Staenz K, Hauff P, Borstad GA (1998) Hyperspectral imagery for mineral exploration: comparison of data from two airborne sensors. In: Proc. of SPIE Vol. 3438. Part of the SPIE Conference on Imaging Spectrometry IV, San Diego, July, 1998

Olthof I, Fraser RH (2007) Mapping northern land cover fractions using Landsat ETM+. Remote Sensing of Environment 1007:496–509

Ontario Wetland Evaluation System: Southern Manual (2002) Ontario Ministry of Natural Resources. NEST Technical Manual TM-002. MNR Warehouse #50254–1. 178p

Ontario Wetland Evaluation System: Southern Manual (2013) Ontario Ministry of Natural Resources. 283 p

Ozesmi SL, Bauer ME (2002) Satellite remote sensing of wetlands. Wetlands Ecology and Management 10:381–402

Pax-Lenney M, Woodcock CE, Macomber SA, Gopal S, Song C (2001) Forest mapping with a generalized classifier and Landsat TM data. Remote Sensing of Environment 77:241–250

Pekel J-F, Vancutsem C, Bastin L, Clerici M, Vanbogaert E, Bartholome E, Defourny P (2014) A near real-time water surface detection method based on HSV transformation of MODIS multi-spectral time series data. Remote Sensing of Environment 140:704–716

Ramsey EW (1998) In: Lunetta RS, Elvidge CD (eds) Radar remote sensing of wetlands in remote sensing change detection: environmental monitoring methods and applications. Sleeping Bear Press, Inc., Chelsea 318p

Rivero RG, Grunwald S, Bruland GL (2007) Incorporation of spectral data into multivariate geostatistical models to map soil phosphorus variability in a Florida wetland. Geoderma 140:428–443

Rogers AS, Kearney MS (2004) Reducing signature variability in unmixing coastal marsh Thematic Mapper scenes using spectral indices. International Journal of Remote Sensing 25:2317–2335

Sabol DE, Gillespie AR, Adams JB, Smith MO, Tucker CJ (2002) Structural stage in Pacific Northwest forests estimated using simple mixing models of multispectral images. Remote Sensing of Environment 80:1–16

Schmid T, Koch M, Gumuzzio J (2005) Multisensor approach to determine changes of wetland characteristics in semiarid environments (Central Spain). IEEE Transactions on Geoscience and Remote Sensing 43:2516–2525

Semlitsch RD, Bodie JR (1998) Are small, isolated wetlands expendable? Conservation Biology 12:1129–1133

Shimabukuro YE, Smith JA (1991) The least-squares mixing models to generate fraction images derived from remote sensing multispectral data. IEEE Transactions on Geoscience and Remote Sensing 29:16–20

Sunderman SO, Weisberg PJ (2011) Remote sensing approaches for reconstructing fire perimeters and burn severity mosaics in desert spring ecosystems. Remote Sensing of Environment 115:2384–2389

Tan Q, Shao Y, Yang S, Wei Q (2003) Wetland vegetation biomass estimation using Landsat-7 ETM+ data. Photogrammetric Engineering & Remote Sensing of Environment 2629-2631

Vermaire JC, Prairie YT, Gregory-Eaves I (2011) The influence of submerged macrophytes on sedimentary diatom assemblages. Journal of Phycology 47:1230–1240

Waleska S, Rodrigues P, Walfir P, Souza-Filho M (2011) Use of multi-sensor data to identify and map tropical coastal wetlands in the Amazon of Northern Brazil. Wetlands 31:11–23

Wright C, Gallant A (2007) Improved wetland remote sensing in Yellowstone National Park using classification trees to combine TM imagery and ancillary environmental data. Remote Sensing of Environment 107:582–605

Yang L, Homer C, Brock J, Fry J (2013) An efficient method for change detection of soil, vegetation, and water in the Northern Gulf of Mexico wetland ecosystem. International Journal of Remote Sensing 34:6321–6336

Zhang SL, Shi JC, Dou YJ (2012) A soil moisture assimilation scheme based on the microwave land emissivity model and community land model. International Journal of Remote Sensing 33:2770–2797

Zoffoli ML, Kandus P, Madanes N, Calvo DH (2008) Seasonal and interannual analysis of wetlands in South America using NOAA-AVHRR NDVI time series: the case of the Parana Delta Region. Landscape Ecology 23:833–848